Observing the Local Emergence of the Southern Ocean Residual-Mean Circulation

F. Sevellec, A. Naveira Garabato, C. Vic, N. Ducousso

Observing the Local Emergence of the Southern Ocean Residual-Mean Circulation

F. Sévellec[1,2], A. Naveira Garabato[2], C. Vic[2], and N. Ducousso[1]

[1]Laboratoire d'Océanographie Physique et Spatiale, CNRS Univ.-Brest IRD Ifremer, Brest, France

[2]Ocean and Earth Science, University of Southampton, Southampton, UK

Key Points.

- Horizontal buoyancy advection by mesoscale eddies at a Southern Ocean mooring site balances mean vertical advection on timescale of 100 days.
- The overturning circulation of the Southern Ocean emerges on this timescale as a residual between the eddy-induced and Eulerian-mean flows.
- The eddy-induced flow can be accurately parameterized with a Gent-McWilliams diffusivity of $\sim$2,000 m^2 s^{-1}.

Abstract

The role of mesoscale turbulence in maintaining the mean buoyancy structure and overturning circulation of the Southern Ocean is investigated through a 2-year-long, single-mooring record of measurements in Drake Passage. The buoyancy budget of the area is successively assessed within the Eulerian and the Temporal-Residual-Mean frameworks. We find that a regime change occurs on timescales of 1 day to 100 days, characteristic of mesoscale dynamics, whereby the eddy-induced turbulent horizontal advec-

tion balances the vertical buoyancy advection by the mean flow. We use these diagnostics to reconstruct the region's overturning circulation, which is found to entail an equatorward downwelling of Antarctic Intermediate and Bottom Waters and a poleward upwelling of Circumpolar Deep Water. The estimated eddy-induced flow can be accurately parameterized via the Gent-McWilliams closure by adopting a diffusivity of $\sim$2,000 m^2 s^{-1} with a mid-depth increase to 2,500 m^2 s^{-1} at 2,100 m, immediately underneath the maximum interior stratification.

1. Introduction

The Southern Ocean plays a pivotal role in the global ocean circulation by connecting the Indian, Pacific, and Atlantic basins [*Schmitz*, 1996], and the ocean's deep and surface layers [*Lumpkin and Speer*, 2007]. The regional circulation is shaped by physical processes acting on a wide range of spatio-temporal scales – from large-scale, persistent Ekman flows, directly linked to surface wind forcing, to meso- and small-scale turbulent motions [*Speer et al.*, 2000]. Assessing the relative contributions of, and interplay between, this spectrum of flows in determining the Southern Ocean limb of the Meridional Overturning Circulation (MOC) remains an important open question, with implications for e.g., global ocean heat uptake [*Liu et al.*, 2018] and sequestration of carbon dioxide [*Landschützer et al.*, 2015]. However, a complete assessment of these dynamics and their effects is outstanding due to the difficulty of rigorously distinguishing between averaged quantities (produced through inaccurate diagnostic) and mixed quantities (produced through actual mixing). Averaged quantities can be likened to the development of a blurred picture in photography when an overly long exposure time is used to capture a moving object. Hence, unlike mixed quantities, they are the outcome of an inaccurate observation rather than a property of the observed system. The erroneous interpretation of averaged quantities as mixed quantities has been rationalized in the context of the time-mean ocean circulation through the Temporal-Residual-Mean (TRM) framework put forward by *McDougall and McIntosh* [2001].

Here, we acknowledge this issue, by examining and quantifying the way in which the mean buoyancy structure and overturning circulation are established at a Southern Ocean

site, where a mooring was deployed for 2 years. This also allows us to estimate the eddy-induced Gent-McWilliams diffusivities. To conclude, a discussion of the impact of our observational results for our understanding and numerical model representation of the Southern Ocean limb of the MOC is provided.

2. Two distinct buoyancy budget regimes

To assess the contributions of motions of different scales to sustaining the extension of the MOC across the Southern Ocean, we used *in situ* observations from a mooring located in the Antarctic Circumpolar Current (ACC) at 56°S, 57°50′W (Fig. 1a), leeward of the Drake Passage [see Fig. 1a and *Brearley et al.*, 2013, for details of the exact location]. These 2-year long measurements were part of a 6-mooring cluster deployed under the auspices of the Diapycnal and Isopycnal Mixing Experiment in the Southern Ocean [DIMES, *Naveira Garabato*, 2010; *Meredith*, 2011]. This study uses co-located horizonal velocity, temperature, salinity and pressure data at 1200-, 1299-, 1853-, 1951-, 2049-, 2152-, 3400-, 3600-m depth (see Text S1 for further details). From these observations, vertical velocities can be inferred, and the terms of a time-mean buoyancy budget can be diagnosed. The method to compute vertical velocities from single-mooring measurements is described in *Sévellec et al.* [2015] and summarized in Text S2; the mean statistical properties of the observational record are shown in Figs. 1b-g. Taking advantage of the equivalent-barotropic nature of the ACC flow [*Killworth and Hughes*, 2002], we defined gradients in the along and across directions of the time- and depth-mean flow (as indicated in Fig. 1a). This enables us to eliminate contributions to the buoyancy budget from the time-mean flow in the across direction (Fig. 1c), except for a small baroclinic component.

Since the measurements were obtained at broadly constant depth levels, it is natural to compute the buoyancy balance in an Eulerian framework with fixed depths. We start from the buoyancy conservation equation:

$$\partial_t b + u\partial_x b + v\partial_y b + w\partial_z b = 0, \tag{1}$$

where t is time; x, y, and z are the along, across, and vertical directions; b is the buoyancy; and u, v, and w are the along, across, and vertical velocities. By applying a Reynolds decomposition, set for a range of averaging periods (from 15 minutes to $\sim$2 years), we separate mean quantities from fluctuations. Taking the overall long-time-mean of this decomposition allows us to build a mean buoyancy budget, which intrinsically depends on the averaging/filtering period (as described in Text S3). This can be expressed in terms of mean and turbulent advection as:

$$\mathrm{Mean}_{\mathrm{hor}}(\tau, z) + \mathrm{Mean}_{\mathrm{ver}}(\tau, z) \simeq \mathrm{Turb}_{\mathrm{hor}}(\tau, z) + \mathrm{Turb}_{\mathrm{ver}}(\tau, z), \tag{2}$$

where τ is the averaging period, $\mathrm{Mean}_{\mathrm{hor}}$ and $\mathrm{Mean}_{\mathrm{ver}}$ are the mean horizontal and vertical advection of buoyancy, and $\mathrm{Turb}_{\mathrm{hor}}$ and $\mathrm{Turb}_{\mathrm{ver}}$ are the turbulent horizontal and vertical advection of buoyancy, respectively. The mean buoyancy budget measures the relative contribution of the turbulent/fluctuation and mean terms in setting the long-time-mean equilibrium. It also shows how these contributions depend on the averaging/filtering period used in the Reynolds decomposition. Note that there is also a trend term in (**??**) compared to (2); however, it is negligible at all depths and for all averaging timescales by construction of the mean buoyancy budget (Text S3).

The resulting buoyancy advective terms are enhanced in the upper part of the measured water column, between 1,000 m and 2,000 m (Fig. 2), where buoyancy gradients, and notably vertical stratification, attain maximum values (Fig. 1). The turbulent vertical advection (Fig. 2d) is negligible at all depths and for all averaging periods. This indicates that variations in vertical velocity and vertical stratification do not correlate highly enough to sustain a net turbulent advection, despite their substantial magnitudes compared to their mean values (Figs. 1d and 1g). In contrast, the mean vertical advection induces a buoyancy gain between 1,000 m and 2,000 m (Fig. 2b). This is consistent with a mean downwelling of buoyant water: a downward mean vertical velocity through a positive vertical stratification. The mean downwelling is robust to changes in averaging period, confirming the steadiness of this buoyancy flux.

The mean horizontal advection induces a buoyancy loss between 1,000 m and 2,000 m for averaging periods shorter than 1 day, but is insignificant for periods longer than $\sim$100 days (Fig. 2a). This dependency to averaging timescale suggests that this term is not sustained by a steady horizontal flow. Finally, the turbulent horizontal advection also induces a buoyancy loss between 1,000 m and 2,000 m (Fig. 2c) that emerges for averaging periods longer than $\sim$1 day, converging to a steady value for periods longer than 100 days. This indicates that variations in horizontal velocity (Fig. 1b and 1c) and in horizontal buoyancy gradients (Fig. 1e and 1f) are significantly correlated on periods between 1 day and 100 days.

The preceding Eulerian buoyancy budget exhibits a remarkable dependence on averaging period. Whereas on short timescales the buoyancy balance is between the mean

horizontal advection and the mean vertical advection ($\text{Mean}_{\text{hor}}+\text{Mean}_{\text{ver}}\simeq 0$), on long timescales it is the turbulent horizontal advection that balances the mean vertical advection ($\text{Mean}_{\text{ver}}\simeq\text{Turb}_{\text{hor}}$). The change in regime occurs between 1-100 days. This timescale is characteristic of mesoscale dynamics, as may be shown e.g., by considering the 6-day propagation timescale derived from the observed zonal propagation speed of mesoscale eddies [2 cm s^{-1}, *Klocker and Marshall*, 2014] and the baroclinic Rossby deformation radius [10 km, *Chelton et al.*, 1998] characteristic of the ACC. Accordingly, variability within this timescale will be referred to as mesoscale turbulence in the remainder of this study [*Klocker and Abernathey*, 2014].

The permanent regime is reached for averaging periods of 100 days. This convergence timescale was reported by *Sévellec et al.* [2015] in a previous investigation of regional dynamics. This period is linked to the cumulative effect of mesoscale eddies propagating over the mooring site, and defines the minimum time over which measurements of eddy variables must be acquired to obtain robust statistics and a convergence of the buoyancy budget. This is symptomatic of the central role of eddies in sustaining the turbulent horizontal advection. On timescales of 100 days, a balance is established between mean vertical advection leading to a buoyancy gain and turbulent horizontal advection inducing a buoyancy loss, in the depth range between 1,000 m and 2,000 m (Fig 2). This is consistent with the prevalent view of the Southern Ocean limb of the MOC equatorward of the ACC's axis, where the mooring is located (i.e., equatorward of the maximum gradient of dynamic ocean topography, Fig.1a). In this area, buoyant waters are expected to be downwelled by the mean vertical circulation; this effect is balanced by the mesoscale ed-

dies inducing a sink of buoyancy at depth [*Toggweiler and Samuels*, 1995, 1998; *Marshall and Radko*, 2003, 2006]. If ergodicity of the ACC flow is assumed (i.e., if time averaging may be considered as equivalent to spatial averaging), our observational diagnostics indicate that mean downwelling at the ACC's northern edge [which represents the equatorward, downwelling branch of the 'Deacon cell', *Döös and Webb*, 1994] is compensated by horizontal mesoscale eddy turbulence.

3. The residual-mean circulation

Having documented the pivotal role of turbulent horizontal advection on timescales longer than 100 days in balancing persistent downwelling, we will test how the former is represented within the TRM framework [*McDougall and McIntosh*, 1996, 2001]. This will enable us to characterize the physical nature of turbulent horizontal advection. In particular, we will assess the extent to which the turbulent buoyancy flux may be accurately parameterized in terms of an adiabatic advection, which has been regularly assumed to prevail over diabatic processes [*Gent and McWilliams*, 1990]. This parameterisation often entails the addition of an eddy-induced velocity proportional to the mean isopycnal slope [*Gent and McWilliams*, 1990]. In assessing this parameterization approach, we will mainly concentrate on the permanent regime (i.e., the longest time average).

We apply the TRM framework and compute the quasi-Stokes velocities, as initially suggested by *McDougall and McIntosh* [1996] and elaborated by *McDougall and McIntosh* [2001], and summarized in Text S4. We obtain the eddy-induced velocities in the along and across directions of the time- and depth-mean flow (respectively referred to as along and across eddy-induced velocities henceforth), and in the vertical direction (Fig. 3a). The

along eddy-induced velocities are small compared to the mean along velocities (Fig. 3a1), indicating that the residual along transport is mainly determined by the intense mean flow along the path of the ACC. For the across direction, the residual velocities (computed as the sum of the mean and eddy-induced velocities) are determined primarily by the eddy-induced velocities, and exhibit a substantial baroclinic structure (Fig. 3a2). This suggests that the residual across transport is dominated by the integrated effect of turbulent processes. In turn, vertical eddy-induced velocities are of similar intensity to the vertical mean velocities (Fig. 3a3). This results in a significant compensation of the mean and eddy-induced vertical velocities at all depths, which leads to the occurrence of small residual vertical velocities (Fig. 3a3). Thus, the vertical transport of buoyancy is significantly weaker than suggested by the mean vertical velocities because of the opposing contribution of eddy-induced flows. This local result is consistent with the common, general circulation model-based view of the residual-mean circulation in the Southern Ocean, in which the Eulerian-mean vertical flow is almost perfectly balanced by the eddy-induced flow [i.e., the vanishing of the Deacon cell in the residual-mean framework, *Döös and Webb*, 1994; *McIntosh and McDougall*, 1996]. Overall, along residual velocities are of the order of tens of centimeters per second, across residual velocities are of the order of centimeters per second, and vertical residual velocities are of the order of tenths of millimeters per second.

Using these eddy-velocities we can express the buoyancy balance within the TRM framework as: Trnd+Hor+Ver=0, where Trnd is the trend of modified buoyancy ($\hat{b}$=$\overline{b}$+$\tilde{b}$, the three terms denoting the modified buoyancy, mean buoyancy, and the rescaled buoy-

ancy variance), Hor=$\hat{u}\partial_x\hat{b}+\hat{v}\partial_y\hat{b}$, and Ver=$\hat{w}\partial_z\hat{b}$ (where $\hat{u}=\overline{u}+\tilde{u}$, $\hat{v}=\overline{v}+\tilde{v}$, and $\hat{w}=\overline{w}+\tilde{w}$ are residual, mean, and eddy-induced along, across, and vertical velocities). Closer examination of this buoyancy balance reveals that the trend of modified buoyancy is small compared to the horizontal and vertical advection of modified buoyancy, which tend to mutually compensate (Fig. 3b1). Vertical and horizontal fluxes of buoyancy are decomposed into four terms, in accordance with the TRM framework of *McDougall and McIntosh* [2001] and as summarized in Text S4. These terms correspond to: mean advection of mean buoyancy (MAM); turbulent advection of mean buoyancy (TAM); mean advection of re-scaled buoyancy variance (MAV); and turbulent advection of re-scaled buoyancy variance (TAV); such that $\mathrm{MAM_{ver}}=\overline{w}\partial_z\overline{b}$, $\mathrm{TAM_{ver}}=\tilde{w}\partial_z\overline{b}$, $\mathrm{MAV_{ver}}=\overline{w}\partial_z\tilde{b}$, and $\mathrm{TAV_{ver}}=\tilde{w}\partial_z\tilde{b}$ (and equivalently for the horizontal terms).

From this diagnostic, we find that the horizontal buoyancy flux is primarily determined by the mean and turbulent advection of mean buoyancy and by the mean advection of re-scaled buoyancy variance, with a negligible contribution of the turbulent advection of re-scaled buoyancy variance (Fig. 3b2). In contrast, the vertical buoyancy flux is dominated by the contribution of the mean and turbulent advection of mean buoyancy, with negligible influence from the mean and turbulent advection of re-scaled buoyancy variance (Fig. 3b3). Note that the vertical advection terms are one order of magnitude larger than their horizontal advection counterparts (Fig. 3b2 vs Fig. 3b3). To summarize, the TRM framework indicates that the mean vertical advection of mean buoyancy and the turbulent vertical advection of mean buoyancy dominate the overall buoyancy balance, and act to compensate one another.

Now that the eddy-induced velocities and associated buoyancy fluxes have been derived and described, we can compute the eddy-induced velocity coefficients required in the *Gent and McWilliams* [1990] parameterisation. The mathematical description of this procedure is summarized in Text S4.

We find that the eddy-induced velocity coefficients for the across direction (relative to the time- and depth-mean flow, as above) range from 500 $m^2\ s^{-1}$ to almost 2,500 $m^2\ s^{-1}$ (Fig. 4a), and vary widely in the vertical. These values including the *Gent and McWilliams* [1990] closure [e.g., 2,000 $m^2\ s^{-1}$ for NEMO in its $2°\times2°$ configuration, *Madec and Imbard*, 1996; *Madec*, 2008], or those diagnosed in regional eddy-resolving models of e.g., the North Atlantic [500 $m^2\ s^{-1}$ and 2,000 $m^2\ s^{-1}$, *Eden et al.*, 2007] or the California Current System [from 300 $m^2\ s^{-1}$ to 750 $m^2\ s^{-1}$, *Colas et al.*, 2013]. Following an abrupt increase from 500 $m^2\ s^{-1}$ at 3,200 m to 1,500 $m^2\ s^{-1}$ at 3,000 m depth, the across coefficient increases linearly up to 2,000 $m^2\ s^{-1}$ at 2,300 m. Directly underneath the maximum deep stratification, the coefficient reaches its peak to values up to 2,500 $m^2\ s^{-1}$ at 2,100 m (Fig. 1g vs Fig. 4a). At shallower levels, the coefficient remains almost constant at 1,800 $m^2\ s^{-1}$ all the way to the upper ocean. Notably, we find that the closure converges when the time-averaging period is increased (Fig. 4a).

4. Discussion and Conclusions

Our analysis of a mooring in the ACC reveals that a regime shift in the buoyancy balance occurs between 1-100 days, associated with the emergence of mesoscale dynamics. A timescale of 100 days characterises the convergence of flow statistics, and corresponds to the minimum time required for enough mesoscale eddy features to propagate past the

mooring. On this and longer timescales, an Eulerian buoyancy budget shows that the mean vertical advection of buoyancy is balanced by turbulent horizontal advection. The latter arises from velocities and buoyancy gradients evolving on timescales ranging from 1 day to 100 days, characteristic of the mesoscale eddy field. The O(1 day) timescale over which the regime change starts can be used to objectively distinguish between the eddying regime and the non-eddying regime in ocean models. Indeed, using an estimate of the speed of first-baroclinic, non-dispersive internal gravity waves (NH/π=0.55 m s^{-1}, where N=1.7×10^{-3} s^{-1} and H=1,000 m following Fig. 1g) and the longest timescale for which the turbulent horizontal advection (i.e., the use of a turbulent closure) is negligible ($1/f \simeq$0.1 day, Fig. 2c), we obtain 0.55×8640=5,000 m or $\sim 1/13^\circ$ at the mooring latitude, which broadly corresponds to the first-baroclinic Rossby deformation radius. This value is significantly smaller than typical horizontal resolutions adopted by global climate models ($\sim 1/4^\circ$ at best) but is close to those used in recent global ocean models ($\sim 1/12^\circ$ at best, except for a few specific studies). This suggests that to accurately represent the buoyancy balance and residual circulation of the Southern Ocean, models require a horizontal resolution of a few kilometres or a robust turbulent closure for the effects of mesoscale eddy flows.

To validate this type of closure against observations, we quantified the eddy-induced circulation through the quasi-Stokes velocities of the TRM framework [*McDougall and McIntosh*, 2001]. We find that the mean horizontal velocities are only weakly modified by the eddy-induced velocities along the direction of the time- and depth-mean flow, whereas eddy-induced velocities dominate for the across direction. This leads to a signifi-

cant residual-mean horizontal transport across the direction of the time- and depth-mean flow (of the order of centimeters per second). In contrast, the mean vertical velocities are strongly compensated by the eddy-induced velocities. This leads to a weak residual-mean vertical transport. The TRM view of the buoyancy balance differs from the Eulerian view. In the former (which distinguishes averaged quantities from mixed quantities, unlike the Eulerian framework), the buoyancy balance is primarily established between the mean vertical advection of mean buoyancy and the turbulent vertical advection of mean buoyancy.

Finally, we considered a parameterization of the eddy-induced circulation as a purely advective process. Following *Gent and McWilliams* [1990], the quasi-Stokes velocity is set proportional to the mean isopycnal slope [computed for the modified buoyancy, *McDougall and McIntosh*, 2001]. This leads to across eddy-induced velocity coefficients of $\sim$2,000 $m^2\ s^{-1}$, but varying by up to a factor 5 over the 2,000-m depth range examined. Our analysis also shows an enhancement of the coefficient up to 2,500 $m^2\ s^{-1}$ at a depth of 2,100 m immediately below the maximum of deep stratification.

All in all, our analysis suggests the existence of a residual-mean circulation that redistributes buoyancy vertically and in the across direction. Mapping the residual-mean flow onto the temperature-salinity relation measured by the moored instrumentation, we can diagnose the motion of the three major water masses present at the mooring location: Antarctic Intermediate Water (AAIW), upper and lower Circumpolar Deep Water (CDW), and Antarctic Bottom Water (AABW). These three water masses are derived from three distinct water types (temperature-salinity properties at their origin/formation):

AAIW defined in the range of 3-7°C and 34.3-34.5 psu [*Carter et al.*, 2009], North Atlantic Deep Water defined in the range of 3-4°C and 34.9-35 psu [*Defant*, 1961], and AABW defined in the range of −0.9-1.7°C and 34.64-34.72 psu by [*Emery and Meincke*, 1986]. Following the density classes set by these three water types, we find that AAIW (lightest layer) flows downward and equatorward, CDW (high-salinity layer) flows upward and poleward, and AABW (densest layer) flows downward and equatorward (Fig. 4b). In this way, the classical description of the large-scale overturning circulation of the Southern Ocean [*Schmitz*, 1996; *Speer et al.*, 2000], derived largely from analyses of basin- or global-scale water mass property distributions and general circulation models, is seen to emerge from local measurements of the buoyancy balance (Fig. 4c).

Acknowledgments. This research was supported by the Natural Environment Research Council of the U.K. through the DIMES (NE/F020252/1) and SMURPHS (NE/N005767/1) projects. ACNG acknowledges the support of the Royal Society and the Wolfson Foundation. FS acknowledges the DECLIC and Meso-Var-Clim projects funded through the French CNRS/INSU/LEFE program.

References

Brearley, J. A., K. L. Sheen, A. C. Naveira Garabato, D. A. Smeed, and S. Waterman (2013), Eddy-induced modulation of turbulent dissipation over rough topography in the southern ocean, *J. Phys. Oceanogr.*, *43*, 2288–2308.

Carter, L., I. N. McCave, and W. M. J. M. (2009), Circulation and water masses of the southern ocean: A review *in* anatractic climate evolution, *Developments in Earth &*

Environmental Science, *8*, 85–114.

Chelton, D. B., R. A. deSzoeke, M. G. Schlax, K. El Naggar, and N. Siwertz (1998), Geographical variability of the first baroclinic rossby radius of deformation, *J. Phys. Oceanogr.*, *28*, 433–460.

Colas, F., X. Capet, J. C. McWilliams, and Z. Li (2013), Mesoscale eddy buoyancy flux and eddy-induced circulation in eastern boundary currents, *J. Phys. Oceanogr.*, *43*, 1073–1095.

Defant, A. (1961), *Physical Oceanography*, 782 pp., Pergmon Press.

Döös, K., and D. J. Webb (1994), The deacon cell and the other meridional cells of the southern ocean, *J. Phys. Oceanogr.*, *24*, 429–442.

Eden, C., R. J. Greatbach, and J. Willebrand (2007), A diagnosis of thickness fluxes in an eddy-resolving model, *J. Phys. Oceanogr.*, *37*, 727–742.

Emery, W. J., and J. Meincke (1986), Global water masses: summary and review, *Oceanologica Acta*, *9*, 383–391.

Gent, P. R., and J. C. McWilliams (1990), Isopycnal mixing in ocean circulation model, *J. Phys. Oceanogr.*, *20*, 150–155.

Killworth, P. D., and C. W. Hughes (2002), The antarctic circumpolar current as a free equivalent-barotropic jet, *J. Mar. Res.*, *60*, 19–45.

Klocker, A., and R. Abernathey (2014), Global patterns of mesoscale eddy properties and diffusivities, *J. Phys. Oceanogr.*, *44*, 1030–1046.

Klocker, A., and D. P. Marshall (2014), Advection of baroclinic eddies by depth mean flow, *Geophys. Res. Lett.*, *41*, 3517–3521.

Landschützer, P., N. Gruber, F. A. Haumann, C. Rödenbeck, S. Bakker, D. C. E. van Heuven, M. Hoppema, N. Metz, C. Sweeney, T. Takahashi, B. Tilbrook, and R. Wanninkhof (2015), The reinvigoration of the southern ocean carbon sink, *Nature*, *349*, 1221–1224.

Liu, W., J. Lu, J.-P. Xie, and A. V. Fedorov (2018), Southern ocean heat uptake, redistribution and storage in a warming climate: The role of meridional overturning circulation, *J. Climate*, pp. doi.org/10.1175/JCLI–D–17–0761.1.

Lumpkin, R., and K. Speer (2007), Global ocean meridional overturning, *J. Phys. Oceanogr.*, *37*, 2550–2562.

Madec, G. (2008), Nemo ocean engine, *Tech. rep.*, Institut Pierre-Simon Laplace (IPSL), France, No27, 332pp.

Madec, G., and M. Imbard (1996), A global ocean mesh to overcome the north pole singularity, *Clim. Dyn.*, *12*, 381–388.

Marshall, J., and T. Radko (2003), Residual-mean solutions for the antarctic circumpolar current and its associated overturning circulation, *J. Phys. Oceanogr.*, *33*, 2341–2354.

Marshall, J., and T. Radko (2006), A model of the upper branch of the meridional overturning of the southern ocean.

Maximenko, N., P. Niiler, M.-H. R̃io, O. Melnichenko, L. Centurioni, D. Chambers, V. Zlotnicki, and B. Galperin (2009), Mean dynamic topography of the ocean derived from satellite and drifting buoy data using three different techniquesp, *J. Atmos. Oceanic Tech.*, *26*, 1910–1919.

McDougall, T. J., and P. C. McIntosh (1996), The temporal-residual-mean velocity. part i: Derivation and scalar conservation equations, *J. Phys. Oceanogr.*, *26*, 2653–2665.

McDougall, T. J., and P. C. McIntosh (2001), The temporal-residual-mean velocity. part ii: Isopycnal interpretation and the tracer and momentum equations, *J. Phys. Oceanogr.*, *31*, 1222–1246.

McIntosh, P. C., and T. J. McDougall (1996), Isopycnal averaging and the residual mean circulation, *J. Phys. Oceanogr.*, *26*, 1655–1660.

Meredith, M. P. (2011), Cruise report: Rrs james cook jc054 (dimes uk2) 30 nov 2010 to 8 jan 2011., *Tech. rep.*, British Antarctic Survey Cruise Rep. 206pp.

Naveira Garabato, A. C. (2010), Cruise report rrs james cook jc041 (dimes uk1) 5 dec 2009 to 21 dec 2009, *Tech. rep.*, National Oceanography Centre Southampton Cruise Rep. 164pp.

Schmitz, W. J. (1996), On the world ocean circulation: Volume ii, *Tech. rep.*, Woods Hole Oceanographic Institution. 237pp.

Sévellec, F., A. C. Naveira Garrabato, J. A. Brearley, and K. L. Sheen (2015), Vertical flow in the southern ocean estimated from individual moorings, *J. Phys. Oceanogr.*, *45*, 2209–2220.

Speer, K., S. R. Rintoul, and B. Sloyan (2000), The diabatic deacon cell, *J. Phys. Oceanogr.*, *30*, 3212–322.

Toggweiler, J. R., and B. Samuels (1995), Effect of drake passage on the global thermohaline circulation, *Deep-Sea Res. Part I*, *42*, 477–500.

346 Toggweiler, J. R., and B. Samuels (1998), On the ocean's large-scale circulation near the
347 limit of no vertical mixing, *J. Phys. Oceanogr.*, *28*, 1832–1852.

Figure 1. (a) Location of the DIMES C-mooring, with red square denoting the location of the 6-mooring cluster. The inset shows a magnification of the region, with blue circle indicating the mooring site. In the main panel, contours represent the dynamic ocean topography averaged from 1992 to 2002 [*Maximenko et al.*, 2009]; the solid thick contour marks −1 m, and solid black and grey contours denote higher and lower values at intervals of 5 cm. Colour represents the absolute gradient of dynamic ocean topography rescaled as horizontal geostrophic velocity magnitude. In the inset, the solid thick contours indicate the 4000 m isobath, and the solid black and grey contours denote shallower and deeper isobaths at intervals of 100 m. The thick blue line shows the time- and depth-averaged direction and magnitude of the flow at the mooring location. This average flow direction defines the along direction used in the remainder of our analysis. The across direction is orthogonal to the along direction. (b) Along, (c) across, and (d) vertical velocities, as well as (e) along, (f) across, and (g) vertical buoyancy gradients at the mooring site. Time-mean values are shown on a uniformly spaced 100-meter vertical grid (black crosses), connected by a cubic-spline interpolation (black line). The red shading represents plus/minus one temporal standard deviation. (Time-mean velocities are also displayed as dashed red lines in Fig. 3a.)

Figure 2. The four components of the buoyancy budget as a function of depth (z) and of the averaging timescale (τ), following (1): (a) mean horizontal advection ($\mathrm{Mean_{hor}}$), (b) mean vertical advection ($\mathrm{Mean_{ver}}$), (c) turbulent horizontal advection ($\mathrm{Turb_{hor}}$), and (d) turbulent vertical advection ($\mathrm{Turb_{ver}}$). Note that $\mathrm{Mean_{hor}}(\tau,z)+\mathrm{Mean_{ver}}(\tau,z)\simeq\mathrm{Turb_{hor}}(\tau,z)+\mathrm{Turb_{ver}}(\tau,z)$. Both depth and averaging timescale axes follow a log scale. (Here the trend is not shown, since Trend$\simeq$0.)

Figure 3. (a1) Along, (a2) across, and (a3) vertical velocities for the (red dashed line) time-mean, (blue dashed line) eddy-induced and (black solid line) residual components for the longest averaging timescale ($\tau=t_2-t_1\simeq2$ years). Eddy-induced velocity is computed through the quasi-Stokes velocity of the Temporal-Residual-Mean framework, and the residual velocity is the sum of the time-mean and eddy-induced velocities. The results are shown on a uniformly spaced 100-meter vertical grid (crosses) and are connected by a cubic spline interpolation (line). (b1-3) Buoyancy budget within the Temporal-Residual-Mean framework as a function of depth for the longest averaging timescale ($\tau=t_2-t_1\simeq2$ years). (b1) Total buoyancy budget between the trend (TRND, black line), horizontal advection (HOR, red line), and vertical advection (VER, blue line). (b2 and b3) Horizontal and vertical buoyancy advection balance between the mean advection of mean buoyancy (MAM, black lines), the turbulent advection of mean buoyancy (TAM, red lines), the mean advection of rescaled buoyancy variance (MAV, blue lines), and the turbulent advection of rescaled buoyancy variance (TAV, purple lines). The results are shown on a uniformly spaced 100-meter vertical grid (crosses) and are connected by a cubic spline interpolation (line).

Figure 4. (a) Coefficients for the Gent-McWilliams turbulent closure for eddy-induced velocities for the across direction. Coefficients are computed for averaging timescales of (blue) 407 days, (red) 679 days and (black) 814 days (i.e., the longest averaging timescale). The mean results are shown on a uniformly spaced 100-meter vertical grid (crosses) and are connected by a cubic spline interpolation (line), with uncertainties (horizontal lines correspond to plus/minus one standard deviation). (b) Temperature-Salinity diagram of the mooring measurements (grey dots) including neutral density at a mean depth of 2,360 m (grey contours) and with the corresponding three water types: Antarctic Intermediate Water (AAIW, red patch), North Atlantic Deep Water (NADW, purple patch), and Antarctic Bottom Water (AABW, blue patch). The residual-mean across and vertical velocities (black arrows) are shown at the location of the time-mean temperature and salinity. Depth of the time-mean temperature is indicated for reference. (c) Schematic of the ocean circulation at the mooring location. A three-layer system is maintained through a balance between buoyancy loss and gain (blue and red arrows, respectively) by horizontal and vertical advection (horizontal and vertical coloured arrows, respectively). This leads to an overall residual-mean circulation of three water masses (black thick arrows) consisting of equatorward downwelling of AAIW and AABW and a poleward upwelling of CDW (Circumpolar Deep Water).

List of Figures

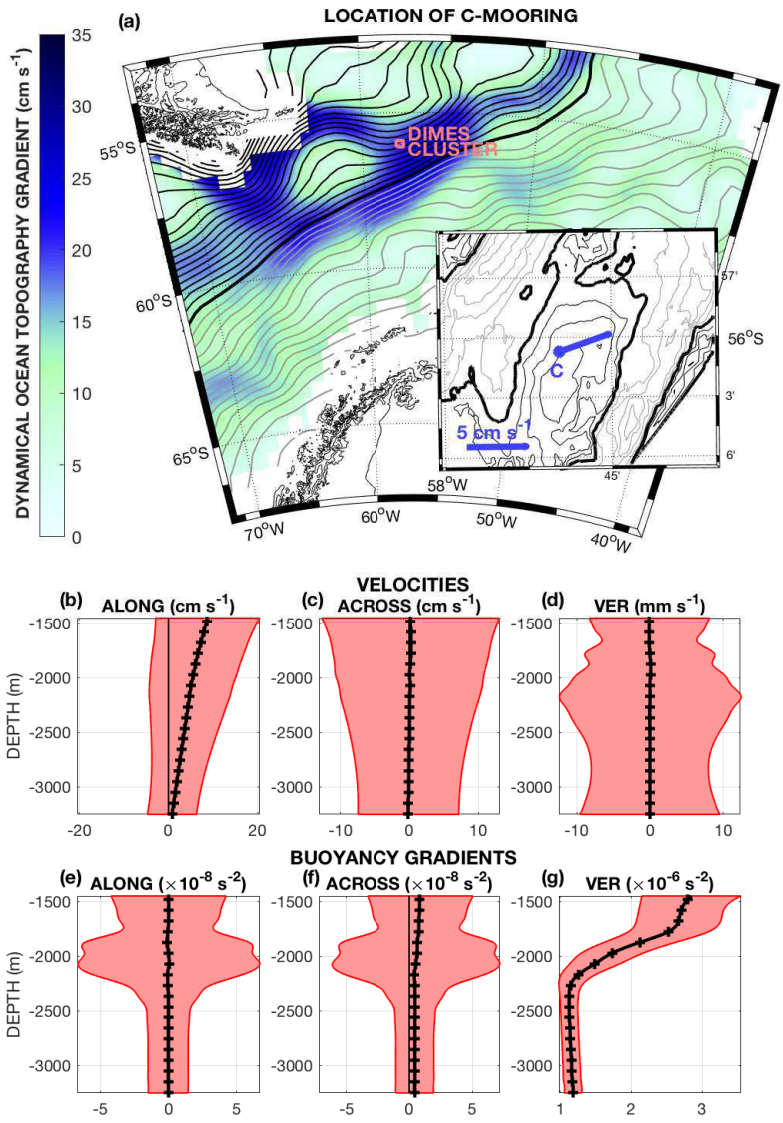

FIGURE 1: (a) Location of the DIMES C-mooring, with red square denoting the location of the 6-mooring cluster. The inset shows a magnification of the region, with black circle indicating the mooring site. In the main panel, contours represent the dynamic ocean topography averaged from 1992 to 2002 [*Maximenko et al.*, 2009]; the solid thick contour marks −1 m, and solid black and grey contours denote higher and lower values at intervals of 5 cm. Colour represents the absolute gradient of dynamic ocean topography rescaled as horizontal geostrophic velocity magnitude. In the inset, the solid thick contours indicate the 4000 m isobath, and the solid black and grey contours denote shallower and deeper isobaths at intervals of 100 m. The thick blue line shows the time- and depth-averaged direction and magnitude of the flow at the mooring location. This average flow direction defines the along direction used in the remainder of our analysis. The across direction is orthogonal to the along direction. (b) Along, (c) across, and (d) vertical velocities, as well as (e) along, (f) across, and (g) vertical buoyancy gradients at the mooring site. Time-mean values are shown on a uniformly spaced 100-meter vertical grid (black crosses), connected by a cubic-spline interpolation (black line). The red shading represents plus/minus one temporal standard deviation. (Time-mean velocities are also displayed as dashed red lines in Fig. 3a.)

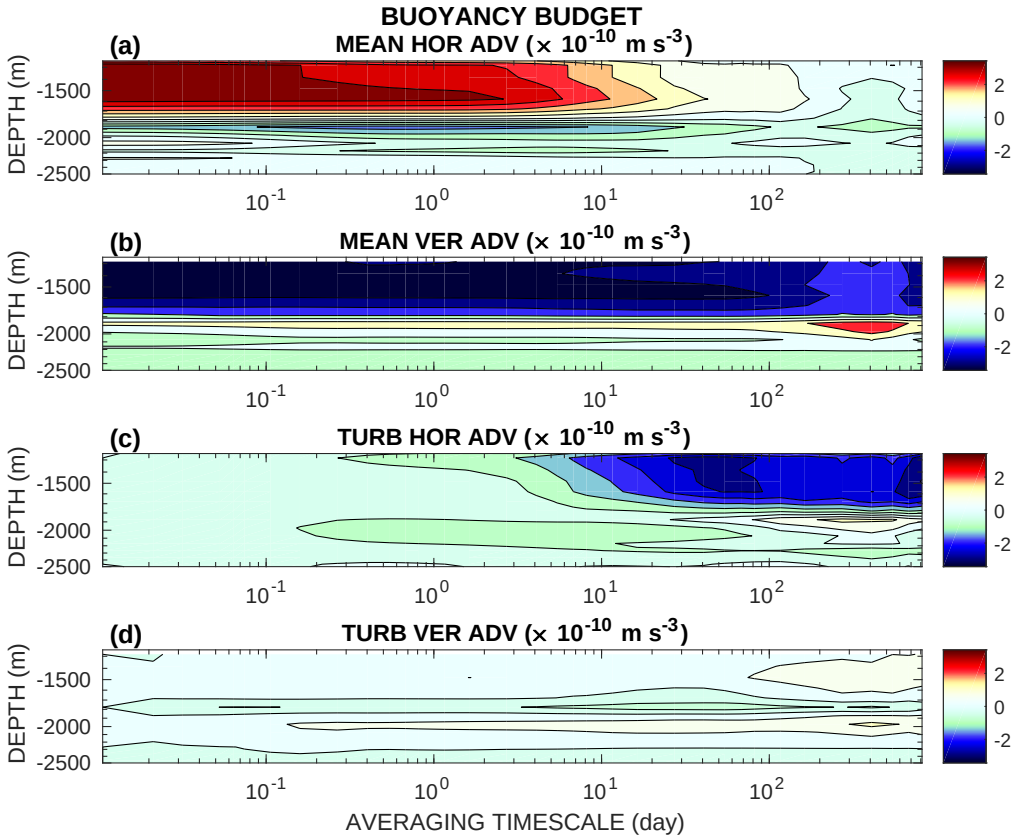

FIGURE 2: The four components of the buoyancy budget as a function of depth (z) and of the averaging timescale (τ), following (1): (a) mean horizontal advection (Mean_{hor}), (b) mean vertical advection (Mean_{ver}), (c) turbulent horizontal advection (Turb_{hor}), and (d) turbulent vertical advection (Turb_{ver}). Note that $\text{Mean}_{\text{hor}}(\tau, z)+\text{Mean}_{\text{ver}}(\tau, z)\simeq\text{Turb}_{\text{hor}}(\tau, z)+\text{Turb}_{\text{ver}}(\tau, z)$. Both depth and averaging timescale axes follow a log scale. (Here the trend is not shown, since Trend$\simeq$0.)

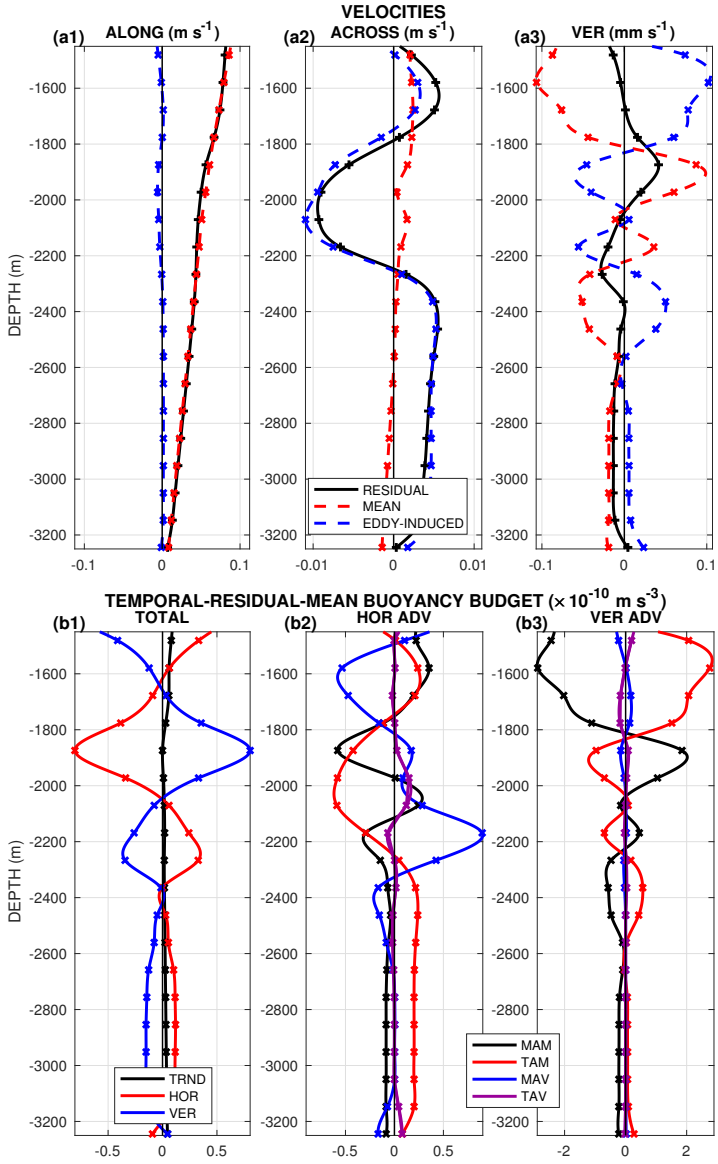

FIGURE 3: (a1) Along, (a2) across, and (a3) vertical velocities for the (red dashed line) time-mean, (blue dashed line) eddy-induced and (black solid line) residual components for the longest averaging timescale (τ=t_2−t_1≃2 years). Eddy-induced velocity is computed through the quasi-Stokes velocity of the Temporal-Residual-Mean framework, and the residual velocity is the sum of the time-mean and eddy-induced velocities. The results are shown on a uniformly spaced 100-meter vertical grid (crosses) and are connected by a cubic spline interpolation (line). (b1-3) Buoyancy budget within the Temporal-Residual-Mean framework as a function of depth for the longest averaging timescale (τ=t_2−t_1≃2 years). (b1) Total buoyancy budget between the trend (TRND, black line), horizontal advection (HOR, red line), and vertical advection (VER, blue line). (b2 and b3) Horizontal and vertical buoyancy advection balance between the mean advection of mean buoyancy (MAM, black lines), the turbulent advection of mean buoyancy (TAM, red lines), the mean advection of rescaled buoyancy variance (MAV, blue lines), and the turbulent advection of rescaled buoyancy variance (TAV, purple lines). The results are shown on a uniformly spaced 100-meter vertical grid (crosses) and are connected by a cubic spline interpolation (line).

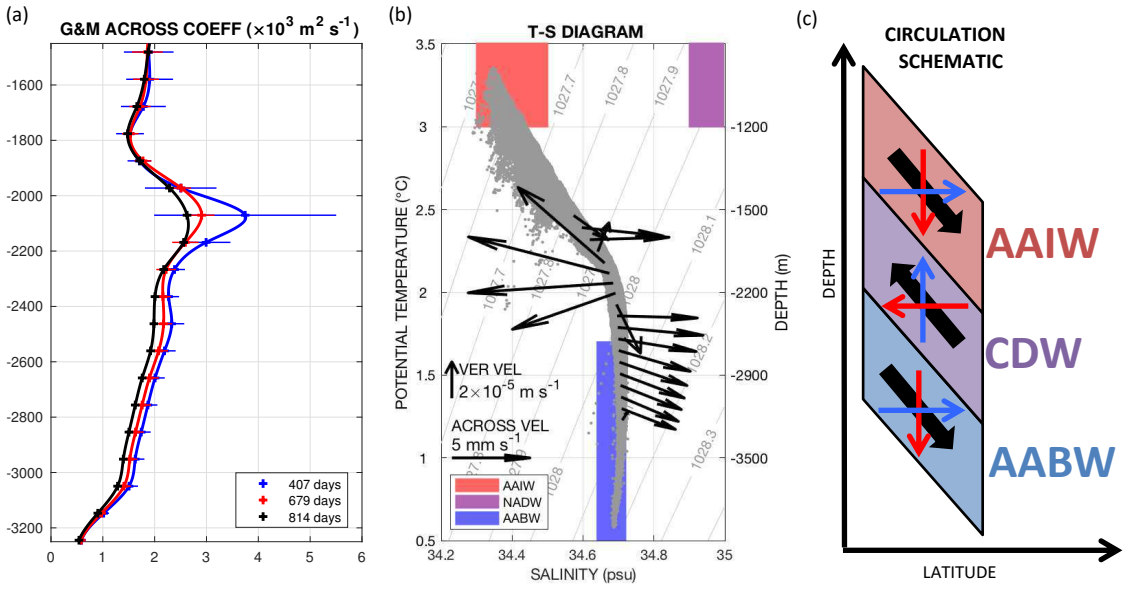

FIGURE 4: (a) Coefficients for the Gent-McWilliams turbulent closure for eddy-induced velocities for the across direction. Coefficients are computed for averaging timescales of (blue) 407 days, (red) 679 days and (black) 814 days (i.e., the longest averaging timescale). The mean results are shown on a uniformly spaced 100-meter vertical grid (crosses) and are connected by a cubic spline interpolation (line), with uncertainties (horizontal lines correspond to plus/minus one standard deviation). (b) Temperature-Salinity diagram of the mooring measurements (grey dots) including neutral density at a mean depth of 2,360 m (grey contours) and with the corresponding three water types: Antarctic Intermediate Water (AAIW, red patch), North Atlantic Deep Water (NADW, purple patch), and Antarctic Bottom Water (AABW, blue patch). The residual-mean across and vertical velocities (black arrows) are shown at the location of the time-mean temperature and salinity. Depth of the time-mean temperature is indicated for reference. (c) Schematic of the ocean circulation at the mooring location. A three-layer system is maintained through a balance between buoyancy loss and gain (blue and red arrows, respectively) by horizontal and vertical advection (horizontal and vertical coloured arrows, respectively). This leads to an overall residual-mean circulation of three water masses (black thick arrows) consisting of equatorward downwelling of AAIW and AABW and a poleward upwelling of CDW (Circumpolar Deep Water).